Review
doi.org/10.1002/open.202100196
Chemistry Europe
European Chemical Societies Publishing

MoS_2-Based Catalysts for N_2 Electroreduction to NH_3 – An Overview of MoS_2 Optimization Strategies

Liang Tian,[a, b] Jinxiu Zhao,[a, b] Xiang Ren,[a, b] Xu Sun,[a, b] Qin Wei,[a, b] and Dan Wu*[a, b]

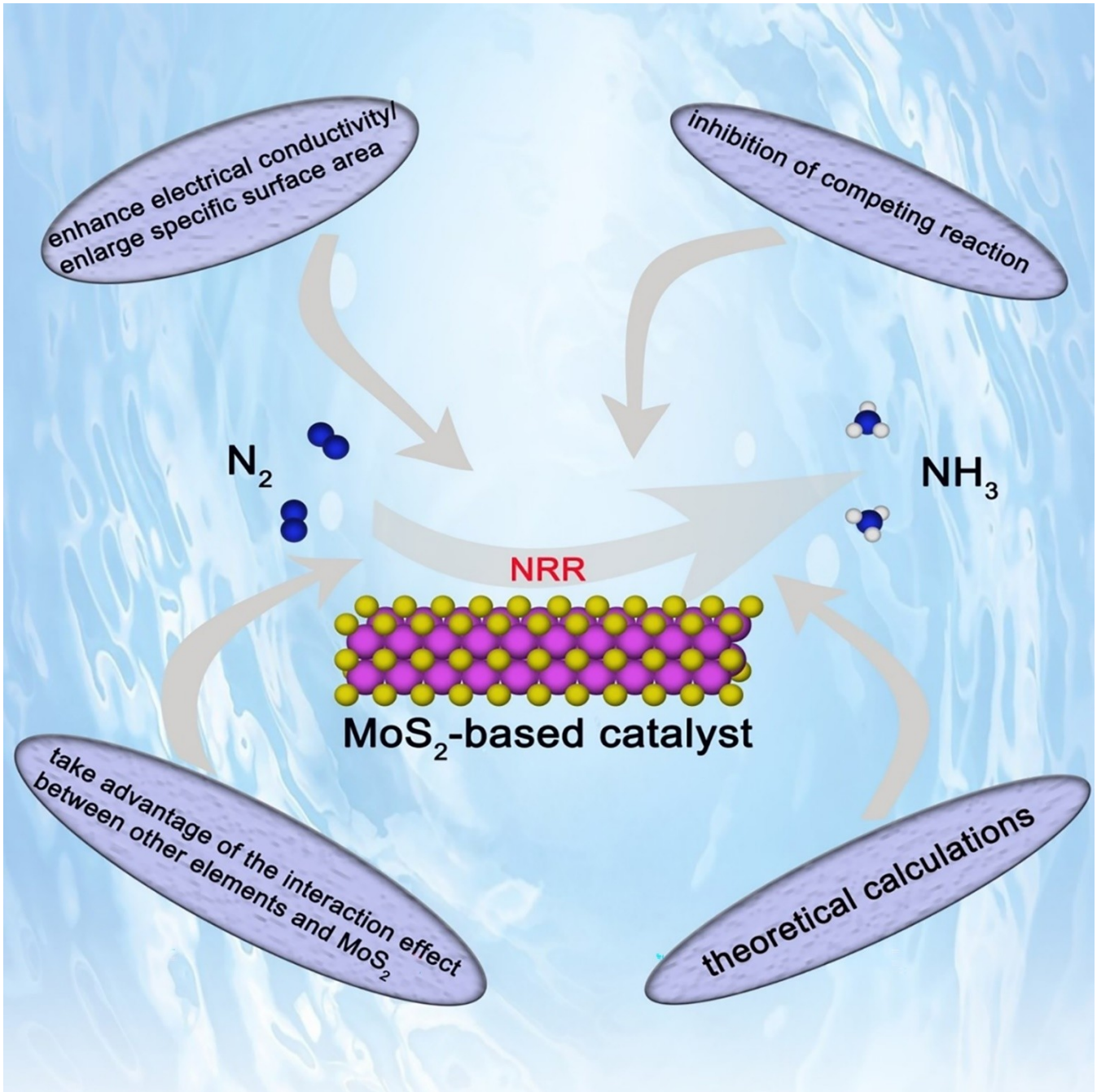

© 2021 The Authors. Published by Wiley-VCH GmbH

The nitrogen reduction reaction (NRR) has become an ideal alternative to the Haber-Bosch process, as NRR possesses, among others, the advantage of operating under ambient conditions and saving energy consumption. The key to efficient NRR is to find a suitable electrocatalyst, which helps to break the strong N≡N bond and improves the reaction selectivity. Molybdenum disulfide (MoS_2) as an emerging layered two-dimensional material has attracted a mass of attention in various fields. In this minireview, we summarize the optimization strategies of MoS_2-based catalysts which have been developed to improve the weak NRR activity of primitive MoS_2. Some theoretical predictions have also been summarized, which can provide direction for optimizing NRR activity of future MoS_2-based materials. Finally, an outlook about the optimization of MoS_2-based catalysts used in electrochemical N_2 fixation are given.

1. Introduction

Ammonia (NH_3) not only plays a significant role in industry, agriculture and other industries related to daily work,[1–4] but also is a potential hydrogen storage material.[5] In industrial production, the Haber-Bosch process is used forNH_3 synthesis. But the Haber-Bosch process has extremely tough requirements, including high temperature (400–500 °C) and pressure (200–250 bar). The process is also accompanied by massive CO_2 emission.[6–9] Therefore, it is urgent to explore a NH_3 synthesis method that has less impact on the environment. Recently, the nitrogen reduction reaction (NRR) has attracted significant attention for artificial N_2 fixation because the NRR process can be performed at ambient conditions and save energy. Hence, it is regarded as an ideal alternative to the Haber-Bosch process.[10–12]

However, the N≡N bond is hard to break (bond energy about 941 kJ mol^{-1}) and the competing hydrogen evolution reaction (HER) has a huge impact.[13] It is thus necessary to identify suitable catalysts to improve the efficiency of ambient NH_3 synthesis. Noble metal catalysts show excellent activity for NRR due to their favorable conductivity and strong chemical binding with reactants.[14–18] But the use of this type of catalyst has been vastly limited by its scarcity. Consequently, numbers of non-noble catalysts have been researched.[19–46] In non-noble catalysts, two-dimensional materials have been widely explored in the NRR field due to the large surface area and novel electronic properties. MoS_2, as an emerging layered two-dimensional material, can conduct electricity like graphene. Compared to other two-dimensional materials, MoS_2 not only has the advantages of adjustable electronic structure, optimal N_2 adsorption energy and good stability in liquid media, but also has the potential of large-scale production as the preparation process is simple. Therefore, it has been largely used in the electrocatalysis field.[47–51]

Recently, Sun and co-workers reported bulk MoS_2 nanosheets for electrochemical N_2 fixation.[52] The nanosheet structure of MoS_2 is markedly displayed in transmission electron microscopy (TEM) images (Figure 1A). In this work, they firstly performed density function theory (DFT) calculations to verify the feasibility of MoS_2 for the NRR process. The calculation results showed that the energy barrier of the potential-determining step (PDS) was 0.68 eV (Figure 1B), which demonstrated MoS_2 was a potential NRR catalyst. The edge of MoS_2 was attested to be the N_2 adsorption site on the basis of Bard charge analysis (a large number of positive charges gather at the edge of MoS_2, as shown in Figure 1C). According to electrochemical experiment, the MoS_2 nanosheet could achieve an NH_3 yield of 8.08×10^{-11} mol s^{-1} cm^{-1} in 0.1 M Na_2SO_4, but the Faraday efficiency (FE) was only 1.17% (Figure 1D), mainly limited by the HER process. Therefore, MoS_2 is indeed a promising and potential NRR electrocatalyst. How to optimize MoS_2 to increase its NRR activity has become a hot topic among researchers.

Herein, we summarize the optimization strategies of MoS_2 since it was first used as a NRR catalyst, including enhancing electrical conductivity/enlarging specific surface area, taking advantage of the interaction effect between other elements and MoS_2 and inhibiting competitive reaction. We also summarize recent theoretical calculations on and predictions of MoS_2-based catalysts. In addition, some advice on how to improve the NRR progress activity of MoS_2-based catalysts is finally presented.

2. The Mechanism of NH_3 Synthesis

The NRR process can be simply divided into the following process: (1) N_2 is adsorbed on the active site of the catalyst surface; (2) to the N atom, hydrogen is constantly added; (3) a NH_3 molecule is released. The mechanism of the NH_3 synthesis process can involve dissociative (Figure 2A) or associative mechanisms (Figures 2B and C). During the pathway of the dissociative mechanism, the N≡N is fractured in advance, then each individual N atom gets hydrogenated. The Haber-Bosch process is thought to follow the dissociative pathway. The associative mechanism can be differentiated in the alternating (Figure 2B) and the distal pathway (Figure 2C) differing in how

[a] Dr. L. Tian, Dr. J. Zhao, Prof. Dr. X. Ren, Prof. Dr. X. Sun, Prof. Dr. Q. Wei, Prof. Dr. D. Wu
Collaborative Innovation Centre for Green Chemical Manufacturing and Accurate Detection School of Chemistry and Chemical Engineering
University of Jinan
Jinan, 250022, Shandong (P.R. China)
E-mail: wudan791108@163.com
[b] Dr. L. Tian, Dr. J. Zhao, Prof. Dr. X. Ren, Prof. Dr. X. Sun, Prof. Dr. Q. Wei, Prof. Dr. D. Wu
Key Laboratory of Interfacial Reaction & Sensing Analysis in Universities of Shandong
School of Chemistry and Chemical Engineering
University of Jinan
Jinan, 250022, Shandong (P.R. China)

© 2021 The Authors. Published by Wiley-VCH GmbH. This is an open access article under the terms of the Creative Commons Attribution Non-Commercial NoDerivs License, which permits use and distribution in any medium, provided the original work is properly cited, the use is non-commercial and no modifications or adaptations are made.

the hydrogenation proceeds. For the alternating pathway, a N atom connects with the surface of the catalyst; followingly, two N atoms are hydrogenated separately until two NH_3 molecules are released. For the distal pathway, the N atom not bound to the catalyst is firstly hydrogenated to release an NH_3 molecule, then the other N atom is hydrogenated and the second NH_3 molecule is released. The adsorption modes of the alternating pathway and the distal pathway are called end-on adsorption.

Another mode of adsorption is called side-on adsorption (Figure 2D). In the side-on adsorption pathway, two N atoms are both bound to the catalyst surface and alternatingly hydrogenated to produce two NH_3 molecules.

3. Strategies for Enhancing the NRR Activity of MoS_2

3.1. Enhancing Electrical Conductivity/Enlarging Specific Surface Area

It has been demonstrated that the edges of MoS_2, that is, free Mo atoms, are the N_2 adsorption sites of MoS_2; thus, creating more active sites to increase N_2 adsorption is beneficial to the improvement of the NRR activity. After MoS_2 had first been used in the electrocatalytic NH_3 synthesis process,[52] Sun and co-workers further used defect-rich MoS_2 nanoflowers as a catalyst for the NRR process.[53] Thanks to the defect structure, the electronic structure of the MoS_2 nanoflowers enhanced the activity of the reaction sites, which was more advantageous to the absorption of N_2. The MoS_2 nanoflowers could achieve a high FE of 20.48% with an NH_3 yield of 29.28 $\mu g\,h^{-1}\,mg_{cat.}^{-1}$ in 0.1 M Na_2SO_4. Liao et al. reported ultra-thin MoS_2 nanosheets with high specific surface area as an NRR catalyst.[54] The large specific surface area leads to an increase in active sites. Therefore, compared with bulk MoS_2, the NH_3 yield of the ultrathin MoS_2 nanosheets achieved a significant growth (41.66 $\mu g\,h^{-1}\,mg_{cat.}^{-1}$), but the FE (1.10%) showed only little improvement due to the strong competing influence of the HER process. Chen et al. employed high temperature annealing to get porous atomic layered MoS_2.[55] Benefiting from the formation of pores, more N_2 adsorption sites on the inert basal plane were exposed. The reasonable use of the inert basal plane of MoS_2 provided a new concept for optimizing MoS_2-base catalysts for NRR. At the same time, the multilayer structure allowed most of the N_2 adsorption sites to take part in the reaction. Thus, an NH_3 yield of 3405.55 $\mu g\,h^{-1}\,mg_{cat.}^{-1}$ and a FE of 44.36% were achieved.

In addition, it is well known that MoS_2 is a semiconductor material,[56] so taking measures to increase MoS_2 electrical conductivity is also an option to optimize the NRR activity of MoS_2-based catalysts. Loading MoS_2 on a suitable substrate is one of the measures to tackle the lack of N_2 adsorption sites and the poor electrical conductivity. As reduced graphene oxide

Liang Tian, graduate student at the Department of Materials and Chemical Engineering of the University of Jinan. His current research focuses on the application of non-noble metal hierarchical heterostructure nanocatalysts for electrocatalytic N_2 reduction reactions.

Jinxiu Zhao received her B.Sc. degree from the University of Jinan in 2017. She is now pursuing her PhD degree at the School of Chemical Engineering of the University of Jinan. Her current research mainly focuses on the electrochemical nitrogen reduction reaction and water splitting.

Xiang Ren received his B.Sc. degree in Chemistry of Materials and English from the University of Jinan in 2012, his M.Sc. degree in Chemical Engineering and Technology from the University of Jinan in 2015, and a PhD degree from the University of Jinan/University of Electronic Science and Technology of China (USTC) in 2019. Now, he is an associate professor at the University of Jinan. His main research interests are energy catalysis, nanomaterial controlled-synthesis, and electrochemical biosensors.

Xu Sun received her PhD in Inorganic Chemistry at the University of Science and Technology of China (USTC). She is now working as an associate professor in the School of Chemistry and Chemical Engineering at the University of Jinan. Currently, her research focuses on the design and fabrication of novel nanomaterials for the construction of energy-related devices.

Qin Wei, a professor and DSc, has devoted herself to analytical teaching and scientific research. Her main research interests are the study of proteins and nucleic acids by photometry and electrochemical immunosensor preparation. She has published over one hundred articles on analysis, immunosensors in journals such as Biomaterials, Adv. Funct. Mater., Biosens. Bioelectron., Sens. Actuators B: Chem., Talanta, and applied successfully for many research projects.

Dan Wu, a professor and DSc, received her PhD degree from Shandong University in 2007.. Her current research focuses on the application of nanomaterials to energy catalysis and sensors.

© 2021 The Authors. Published by Wiley-VCH GmbH

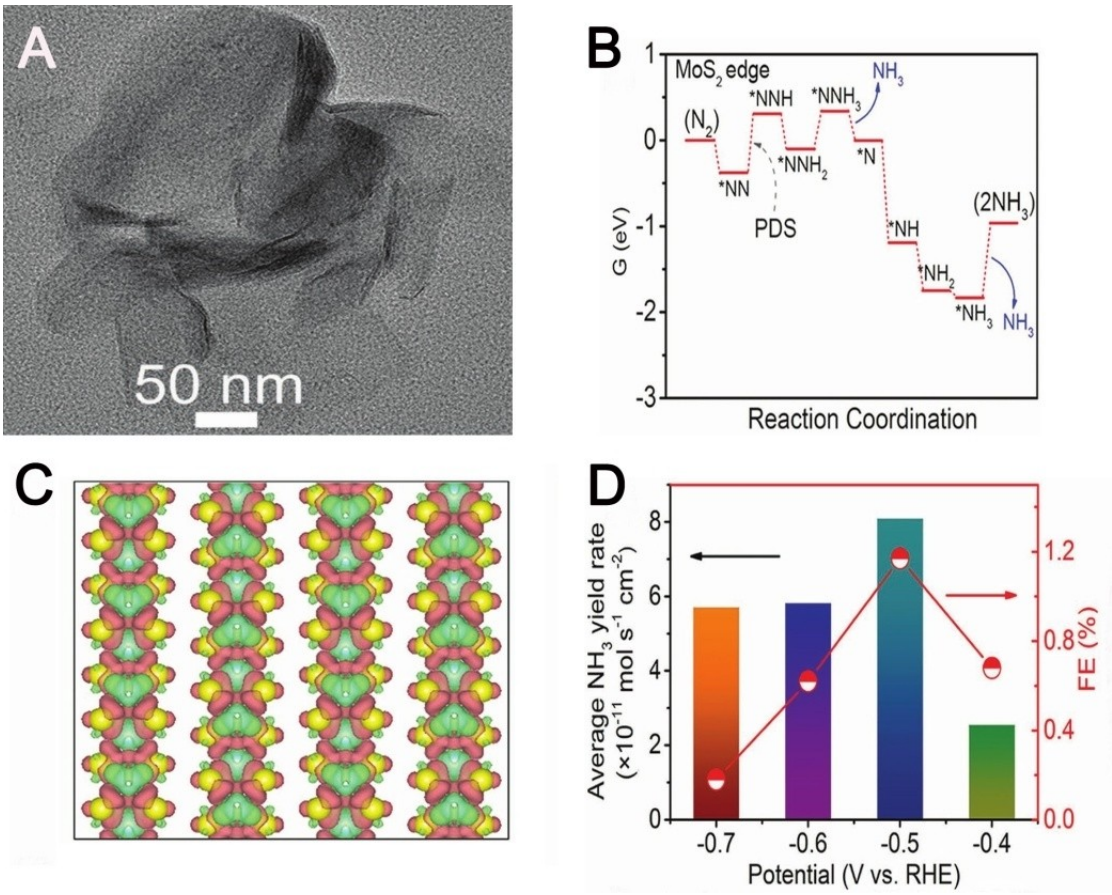

Figure 1. (A) The transmission electron microscope image of MoS_2 nanosheets. (B) Free energy profile proposed by DFT calculations. The asterisk (*) denotes the N_2 adsorption site. (C) The view from atop the isosurface of deformation charge density. Red and green represent charge accumulation and drop at the edge of Mo atoms, respectively. Isosurface is 0.0025 a.u. (D) The NH_3 yields and FE of MoS_2/CC (carbon cloth) at various potentials. Reproduced with permission from Ref. [52]. Copyright 2018 Wiley-VCH.

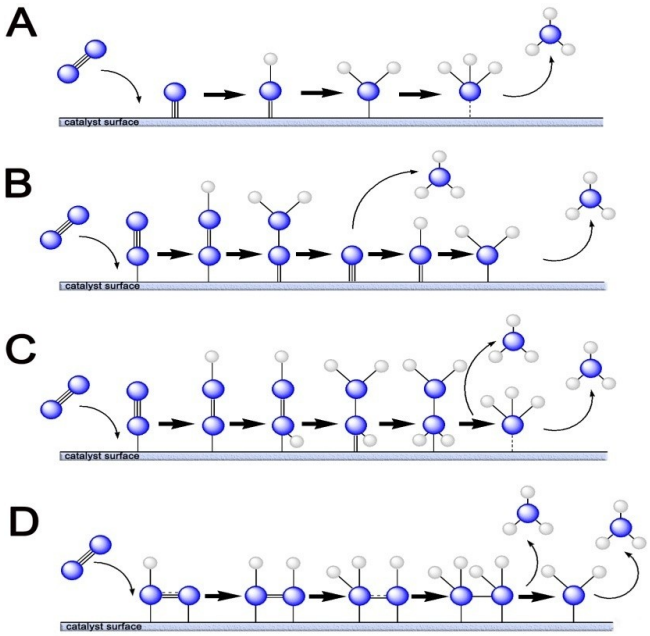

Figure 2. The NRR mechanisms on the surface of catalyst: (A) dissociative pathway; (B) alternating pathway; (C) distal pathway; (D) side-on adsorption. Blue, white represent N, H atoms, respectively.

(rGO) has the advantages of high specific surface area, favorable electroconductibility and high stability, rGO has been widely used in electrocatalysis in recent years.[57] In our recent work, we loaded MoS_2 nanosheets onto rGO to improve the specific surface area and electrical conductivity of MoS_2.[58] Having the reaction taking place in 0.1 M $LiClO_4$ furthermore had the effect of inhibiting the HER (the mechanism will be described specifically in strategy 3.3). Under the synergistic effect of the above strategies, we obtained an NH_3 yield of 24.82 $\mu g\,h^{-1}\,mg_{cat.}^{-1}$ and a FE of 4.56%. As MoS_2 nanodots has the advantages of more N_2 adsorption sites and larger specific surface area compared to nanosheet structures, Zhang and co-workers loaded MoS_2 nanodots uniformly on rGO.[59] By means of X-ray photoelectron spectroscopy (XPS), the MoS_2 nanodots/rGO material was demonstrated to contain strong C–S–C bonds which effectively promoted electron transfer. Thus, MoS_2 nanodots/rGO exhibited a FE of 27.93% at −0.35 V versus the reversible hydrogen electrode (RHE) potential with an NH_3 yield of 16.41 $\mu g\,h^{-1}\,mg_{cat.}^{-1}$ at −0.75 V (vs. RHE).

Through a pyrolysis strategy, Zhao et al. generated MoS_2 grown, in situ, on a C_3N_4 layer, which led to an NH_3 yield of 19.86 $\mu g\,h^{-1}\,mg_{cat.}^{-1}$ with a FE of 6.87%.[60] The reason for the high catalytic activity is the strong interaction between C_3N_4

© 2021 The Authors. Published by Wiley-VCH GmbH

and MoS_2, formed by interfacial Mo–N coordination to promote electron transmission. In addition, the source of N_2 was also determined in electrochemical experiments. They demonstrated that C_3N_4 had no catalytic capacity for NRR, so the N source for electrocatalytic NH_3 synthesis only came from the N_2 in the air. Shao and co-workers immobilized 1T-MoS_2 on g-C_3N_4 (1T-MoS_2/g-C_3N_4) to boost NRR activity.[61] The 1T phase (comprised of edge-sharing [MoS_6] octahedra) had the advantage of more N_2 adsorption sites along the plane and higher electron conductivity than other phases of MoS_2.[62] Therefore, an appropriate load of 1T-MoS_2 was conducive to the adsorption and activation of N_2. 1T-MoS_2/g-C_3N_4 achieved a high catalytic efficiency of NRR (29.97 $\mu g\,h^{-1}\,mg_{cat.}^{-1}$, 20.48 %).

Mao et al. first prepared *n*-butyl triethyl ammonium bromide functionalized polypyrrole/graphene oxide (BTAB/PPy/GO) as a precursor,[63] in which the substrate polypyrrole/graphene oxide was used to enhance electroconductibility and to expand the specific surface area of the catalyst. Interestingly, BTAB/PPy/GO itself showed little NRR activity (Figure 3A), but it did affect the morphology and phase of 1T-MoS_2. 1T-MoS_2/BTAB/PPy/GO (schematic synthesis is shown in Figure 3C) thus could attain a high NRR activity (13.60 $\mu g\,h^{-1}\,mg_{cat.}^{-1}$, 1.96 %). However, after long-term use, the metastable 1T-MoS_2 was transformed into Mo_2N due to the electrochemical reaction with N_2. Having formed new Mo–N bonds, this prevented the catalyst from binding N_2. Figure 3B shows the concentration of NH_4^+ versus operation time; the concentration of NH_4^+ stayed steady after 18 h of reaction, which indicated that the active sites of 1T-MoS_2/BTAB/PPy/GO had been deactivated.

Xu et al. anchored 1T-MoS_2 on Ti_3C_2 MXene through a hydrothermal reaction.[64] Because the 1T-MoS_2 could be fully loaded on the Ti_3C_2 MXene, in turn exposing more N_2 adsorption sites and the composite had high electrical conductivity, the 1T-MoS_2/Ti_3C_2 MXene achieved an NH_3 yield of 30.33 $\mu g\,h^{-1}\,mg_{cat.}^{-1}$ and a FE of 10.94 % in 0.1 M HCl.

3.2. Taking Advantage of the Interaction Effect Between Other Elements and MoS_2

As the NRR performance of MoS_2 is not satisfactory, taking advantage of the interaction effect between other elements and MoS_2 to enhance the NRR activity of MoS_2 has become a widely studied strategy. The interaction effect, including synergy effects and the addition of other elements, can change the electronic structure of MoS_2; thus, heteroatom doping has become the priority approach in this strategy. Zeng et al. achieved a high NH_3 yield of 128.17 $\mu g\,h^{-1}\,mg_{cat.}^{-1}$ and a FE of 11.34 % by doping bimetallic Ni-Fe in MoS_2.[65] The reason for the high activity was that the bimetallic dopant reacted with the S atoms to generate a nanohollow structure (Figure 4A), affording more N_2 adsorption sites because of the synergistic effect of the S-Fe-Ni system. As shown in Figure 4B, Zhao et al. doped a carefully balanced amount of Fe nanodots into MoS_2, using carbon cloth as a substrate, so that the Fe atoms would

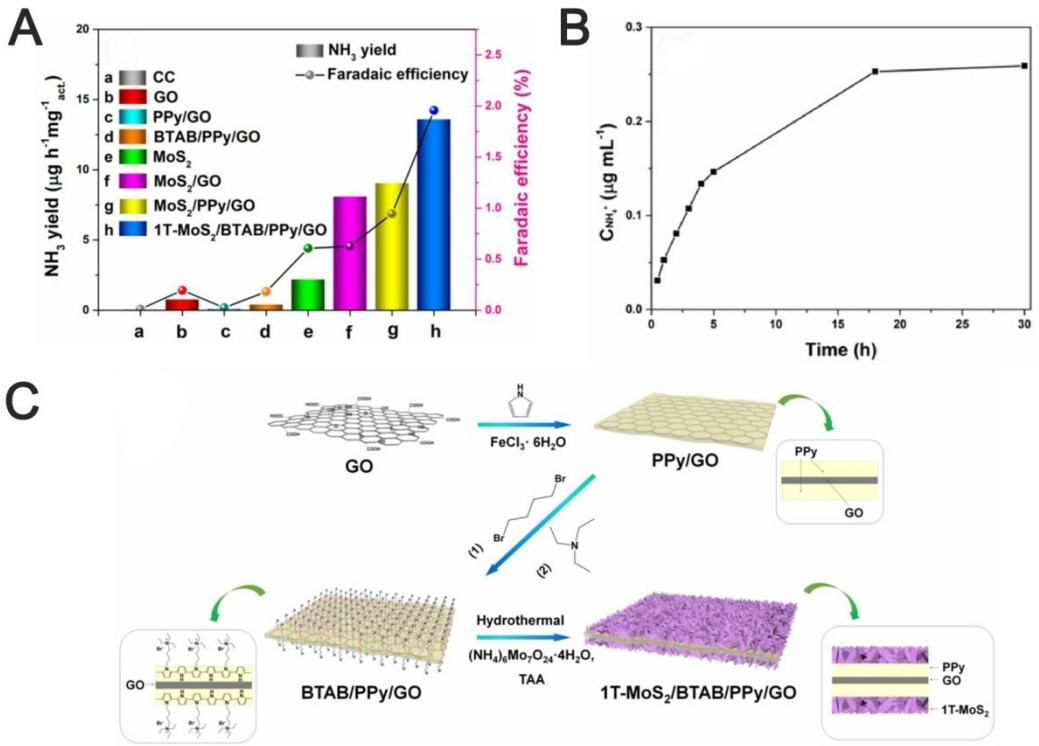

Figure 3. (A) The NH_3 yield and FE of different catalysts at −0.49 V after electrolysis (2 h): (a) carbon cloth (CC), (b) graphene oxide (GO), (c) PPy/GO (PPy = polypyrrole), (d) BTAB/PPy/GO (BTAB = n-butyl triethyl ammonium bromide), (e) MoS_2, (f) MoS_2/GO, (g) MoS_2/PPy/GO and (h) 1T-MoS_2/BTAB/PPy/GO. (B) Time-dependent concentration of NH_4^+ over 30 h in 0.1 M KOH. (C) Schematic synthesis of 1T-MoS_2/BTAB/PPy/GO. Reproduced with permission from Ref. [63]. Copyright 2020 American Chemical Society.

© 2021 The Authors. Published by Wiley-VCH GmbH

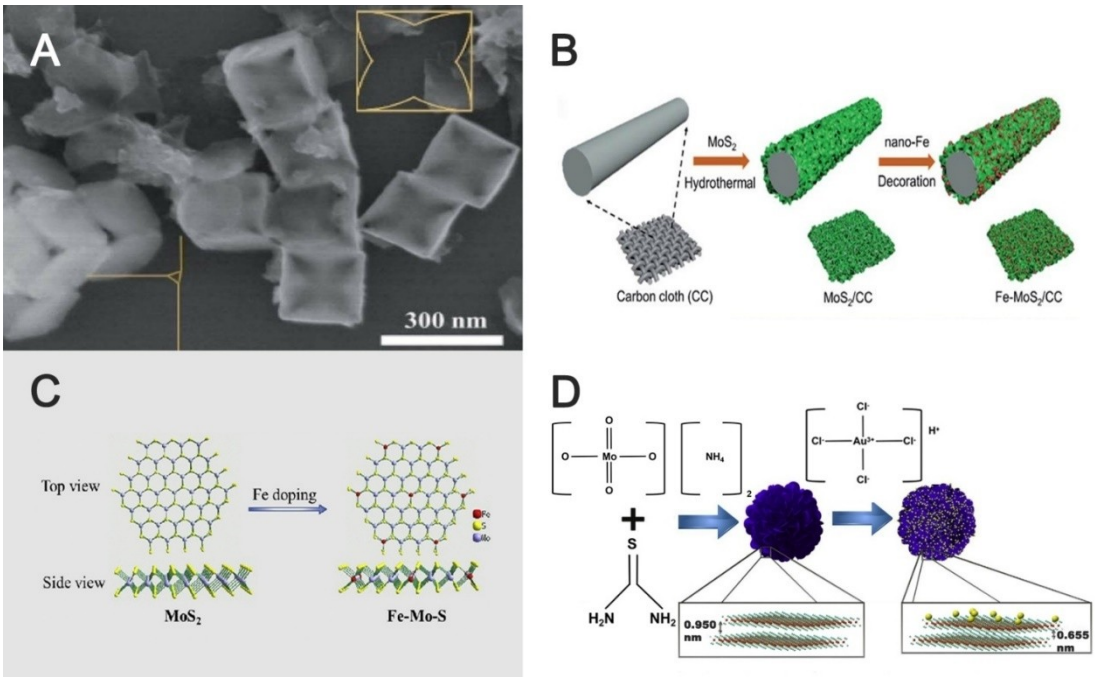

Figure 4. (A) Scanning Electron Microscope (SEM) image of Ni-Fe@MoS_2 nanocubes. Reproduced with permission from Ref. [65]. Copyright 2020 Royal Society of Chemistry. (B) Illustration of the synthesis of Fe-MoS_2/CC. Reproduced with permission from Ref. [66]. Copyright 2019 Royal Society of Chemistry. (C) Structure diagrams of 2H-MoS_2 and Fe-Mo-S materials. Reproduced with permission from Ref. [67]. Copyright 2020 Elsevier. (D) Schematic synthesis of MoS_2 and AuNPs@MoS_2 nanosheets. Modified with permission from Ref. [68]. Copyright 2019 Elsevier.

not aggregate and degrade during the NRR process.[66] The synergistic effect (Fe nanodots can regulate the chemical state of MoS_2) made Fe-MoS_2/CC afford an NH_3 yield of 12.5 $\mu g\,h^{-1}\,cm^{-2}$ with a FE of 10.8%.

Most of the current MoS_2 synthesis processes involve ammonium ions, which leads to unclear N sources in the NRR process. Partially replacing S atoms in 2H-MoS_2 with Fe atoms (Figure 4C), Guo et al. used an ammonium-free hydrothermal process to grow Fe@2H-MoS_2 on carbon cloth,[67] thus successfully avoiding the problem of unclear N sources. The substituted Fe atoms affected the electronic state of Mo and S atoms, which facilitated the adsorption of N_2. Therefore, compared with bulk MoS_2, the NH_3 production rate of Fe@2H-MoS_2 was increased by 10 times and the FE was increased by 5 times.

Since MoS_2 is a semiconductor material, which hinders the process of electron transfer, doping with a conductive metal is a potential strategy of resolving this. In addition to iron-doping, other elements have also been used to produce outstanding results with this strategy. Recently, Zhang et al. have grown ultra-small Au nanoparticles (NPs) on MoS_2 nanosheets to enhance the electron transfer ability of MoS_2 (Figure 4D).[68] They found that the Au on the surface of MoS_2 caused unsatisfied valences, thus adjusting the electronic structure of MoS_2s so as to enhance the absorption of N_2. This, in turn led to an increased NRR activity with an NH_3 yield of 25 $\mu g\,h^{-1}\,mg_{cat.}^{-1}$ and a FE of 9.7%. Suryanto et al. modified 2H-MoS_2 with Ru clusters, producing an electrocatalytic material for the NRR process which achieved an NH_3 yield rate of 1.14×10^{-10} $mol\,cm^{-2}\,s^{-1}$ with a FE of 17.6% (50 °C).[69] The high NRR activity was ascribed to the synergistic interaction between the isolated sulfur vacancies on MoS_2 (the hydrogenation centers) and the Ru cluster (the sites of N_2 binding).

In addition, MoS_2 has also been doped with some non-metals that have also been proven to promote electron transfer. Yang et al. synthesized C/MoS_2 porous nanospheres by a simple one-pot hydrothermal method.[70] Benefitting from the synergistic effect between C and MoS_2, the electron transfer during the N_2 electroreduction to NH_3 was significantly improved. The C/MoS_2 material thus achieved a FE of 8.2%. Zeng et al. reported an impressive NH_3 yield of 69.82 $\mu g\,h^{-1}\,mg_{cat.}^{-1}$ and a high FE (9.14%) by doping N atoms (by using ammonium fluoride during the synthesis) into MoS_2 nanoflower structures.[71] The N atoms altered the electronic structure of MoS_2 and produced abundant S vacancies, which promoted electron transfer.

Due to the appropriate orbital energy and symmetry, the unoccupied and occupied d orbitals of the transition mental (TM) can separately receive electrons from and feed electrons back to the N_2 antibonding orbitals, respectively, activating the N–N bond. Based on this mechanism, Guo et al. proposed a concept of the strong-weak electron polarization (SWEP) pair,[72] consisting of two catalytic centers with vastly different electron acceptance and back-feeder abilities. As the d orbitals of transition metals and the p orbitals of boron show similar behavior, SWEP pairs were created by filling the S vacancy in MoS_2 with B atom (adjusting the electronic structure of MoS_2). The SWEP pair in B–MoS_2/CFC (CFC = carbon fiber cloth) polarized the non-polar N–N bond (Figure 5A), thus promoting

© 2021 The Authors. Published by Wiley-VCH GmbH

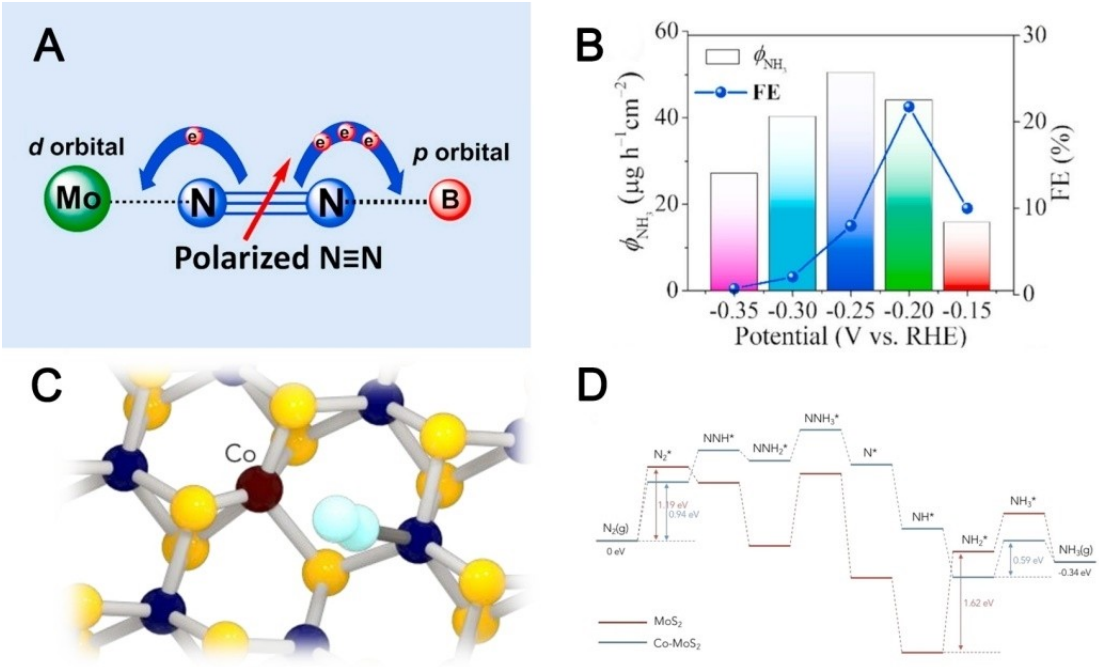

Figure 5. (A) The synergistic polarization of N≡N bond by boron/molybdenum hybrid catalysts in the step of dinitrogen adsorption: strong-weak electron polarization (SWEP). (B) NH_3 yields and FE of B–MoS_2 under different potentials. Reproduced with permission from Ref. [72]. Copyright 2020 Elsevier. (C) Schematic depiction of Co-doped defected MoS_{2-x} with adsorbed N_2. The N_2 molecule (light blue spheres) binds to three Mo atoms (dark blue spheres) near the S (yellow spheres) vacancy position. With Co (dark red sphere) replacing Mo in the catalyst, N_2 binds only one of the remaining Mo atoms near the S vacancy. (D) Free energy profile of NH_3 synthesis at defected MoS_{2-x} (red) and Co-doped MoS_{2-x} (blue) basal planes. Reproduced with permission from Ref. [75]. Copyright 2019 American Chemical Society.

the breaking of the first bond of N≡N. B–MoS_2/CFC thus achieved an NH_3 yield of 44.09 $\mu g\,h^{-1}\,mg_{cat.}^{-1}$ with a FE of 21.72% (Figure 5B).

Besides heteroatom doping, compound loading is also one of the strategies to optimize the NRR activity of MoS_2. Guo et al. reported FeS@MoS_2 under the action of independent conductive substrate carbon fiber cloth (CFC) as an NRR catalyst.[73] The high NRR activity (NH_3 yield of 8.45 $\mu g\,h^{-1}\,cm^{-2}$) of FeS@MoS_2/CFC was ascribed to the synergistic effect arising from FeS nanoparticles providing a large number of N_2 adsorption sites. Yang et al. loaded CoS_2 nanoparticles onto MoS_2 nanosheets as a heterostructured catalyst.[74] The strong interaction between CoS_2 and MoS_2 can adjust the interface charge distribution, which effectively promoted the adsorption of N_2. Thus CoS_2/MoS_2 attained an NH_3 yield of 54.7 $\mu g\,h^{-1}\,mg^{-1}$ and a FE of 20.8%.

Inspired by the role of dinitrogenase in biological NH_3 synthesis, Zhang et al. simulated the active site of nitrogenase by introducing Co atoms to the S vacancy of the MoS_2 basal plane(Figure 5C).[75] The S vacancy could make Mo atoms below the basal plane manifest to generate more N_2 adsorption sites. The energy barrier of the rate-limiting step (Figure 5D), according to DFT calculations, changed from −1.62 eV (MoS_2) to −0.59 eV (Co–MoS_{2-x}), which further proved that Co-doping could enhance the activity of the NRR process. Thus the catalyst could achieve an NH_3 yield over 0.6 $mmol\,h^{-1}\,g^{-1}$ and a FE over 10%. Similar to the work of Zhang et al.,[75] Zeng et al. also prepared Co–MoS_2 by making use of the positive interaction between Co and S.[76] The difference was that they loaded Co–MoS_2 onto a zeolitic imidazolate framework (ZIF) as a heterojunction catalyst, which could benefit from the inhibitory effect of ZIF on the HER process. They further designed a N_2 diffusion cathode because N_2 has a low solubility in the electrolyte. Through the bidirectional optimization of the electrocatalyst and the reaction environment, the Co–MoS_2 could obtain a satisfactory NRR activity in 0.1 M Na_2SO_4 (127.88 $\mu g\,h^{-1}\,mg_{cat.}^{-1}$, 11.29%).

Zheng et al. embedded Fe atoms in single-molecular layered MoS_2 (sMoS_2) which then contained a [Fe–S_2–Mo] motif similar to the core structure of the Fe–Mo–S cluster in nitrogenase. Benefitting from the interactions in the Fe–S_2–Mo motif, Fe–sMoS_2 could achieve an NH_3 yield of 24 $\mu g\,cm^{-2}\,h^{-1}$ with a FE of 27% in 0.5 M K_2SO_4.[77]

Due to the structure of MoS_2, some research has shown that heteroatom doping can also inhibit competing reactions of the NRR process; more detail will be given in the next section.

3.3. Inhibiting Competitive Reaction

As the reaction potentials of the hydrogen evolution reaction (HER) and NRR are similar to each other,[78,79] HER is the biggest competitive reaction in electrocatalytic N_2 reduction. In the original experiment by Sun et al.,[52] it was the influence of the HER that caused the low FE of the pure MoS_2 nanosheets. Therefore, inhibition of the HER process became

© 2021 The Authors. Published by Wiley-VCH GmbH

one of the most effective strategies to enhance the NRR activity. Liu et al. used the interaction between Li and S to inhibit the HER process.[80] Specifically, when S-rich MoS_2 nanosheets were used as NRR catalyst in a 0.1 M Li_2SO_4 electrolyte, the adsorption free energy of H was reduced (0.03 eV→0.47 eV) due to the interaction between Li^+ and the S edge site in MoS_2 (Figure 6A). Thus, the adsorption process of $H^•$ was inhibited. At the same time, the strong action of Li positively charged the edge site of MoS_2, which enhanced adsorption of N_2 (the N_2 adsorption free energy was increased from −0.32 eV to −0.70 eV). Compared to conducting the experiment in a 0.1 M Na_2SO_4 electrolyte, the Li-based electrolyte led to a high NRR activity of the S-rich MoS_2 nanosheets (43.4 $\mu g\, h^{-1} mg_{cat.}^{-1}$, 9.81 %) (Figure 6B). Through electrochemical experiments, Liu et al. verified the stability of the catalyst (Figure 6C and D). In our recent work (mentioned in section 2.1),[58] the Li–S interaction was also used to suppress the HER process. Similarly, in a 0.25 M Li_2SO_4 electrolyte, Patil et al. grew 1T-MoS_2 on nickel foil (1T-MoS_2/NF) for use in the electrochemical N_2 reaction,[81] also using the strong Li–S interaction to inhibit the HER process. In addition, 1T-MoS_2/NF featured pseudo-six-membered rings, in which the interaction between N and Li could enhance the adsorption capacity of N_2. This work provided researchers with a new idea to design N_2 fixation catalysts. 1T-MoS_2/NF reached a FE of 27.66 % and an NH_3 yield of 1.05 $\mu g\, min^{-1} cm^{-2}$.

In this strategy, the above-detailed reports used the action of electrolyte to inhibit the HER process. In addition, optimizing the structure of MoS_2 to inhibit the HER process has also been studied. Su et al. dispersed Fe atom on MoS_2 nanosheets to simulate nitrogenase-like NH_3 synthesis with superior NRR

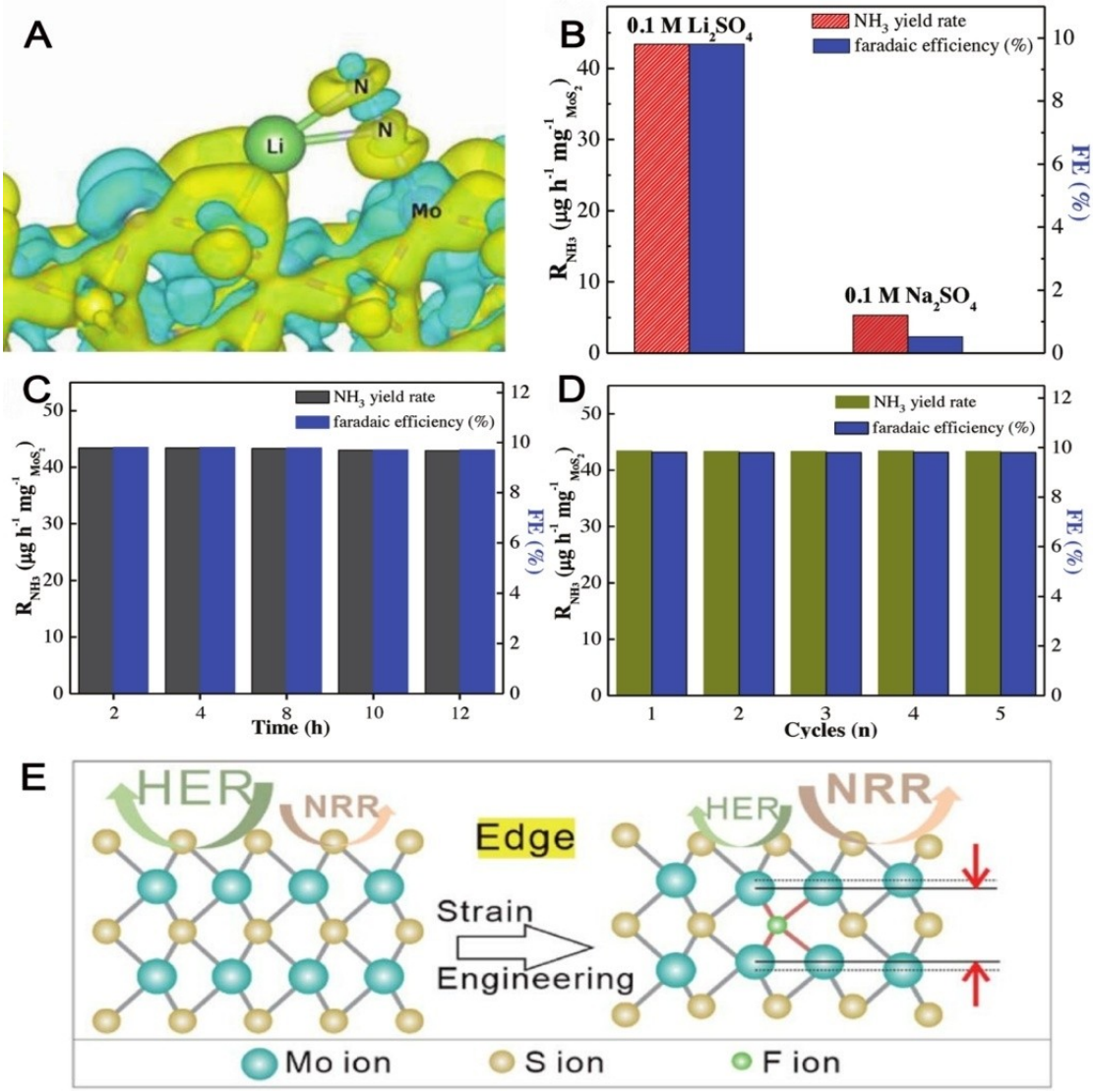

Figure 6. (A) The Li–S interactions as signified by the deformation charge density of $*N_2$ at a MoS_2 edge. Yellow and blue represent charge accumulation and loss, respectively. (B) NH_3 yield and FE of MoS_2/BCCF acquired for N_2-saturated 0.1 M Li_2SO_4 and 0.1 M Na_2SO_4 electrolytes at −0.2 V (vs. RHE) after electrolysis for 2 h. (C) NH_3 yield and FE for a continuous reaction over 12 h. (D) NH_3 yield and FE during a reusability test comprising five cycles of 2 h each. Reproduced with permission from Ref. [80]. Copyright 2019 Wiley-VCH. (E) A sketch map of strain engineering by replacing S on the edge site of the MoS_2 with F. Blue, yellow, green represent Mo, S, F ions, respectively. Reproduced with permission from Ref. [83]. Copyright 2020 Royal Society of Chemistry.

© 2021 The Authors. Published by Wiley-VCH GmbH

activity (8.63 μg h^{-1} $mg_{cat.}^{-1}$, 18.8 %).[82] They modified the S edge position in MoS_2 with Fe atoms, which effectively inhibited the HER process by increasing the energy barrier of HER from 0.03 eV to 0.15 eV.

It is well known that MoS_2 possesses a layered two-dimensional (2D) graphene-like structure and the decrease of MoS_2 layer spacing is beneficial to the inhibition of the HER process. By substituting S with F atoms in defect-rich MoS_2, Liang et al. reported F-MoS_2 as electrocatalyst for the NRR process (Figure 6E).[83] Compared with sulfur, fluorine has a smaller size and higher electronegativity, leading to a decreased layer spacing of MoS_2 and thus reduced HER activity. In addition, this work centered on defect-rich MoS_2 with marginal defects (larger specific surface area than bulk MoS_2), which further increased the number of active sites for N_2 fixation. Therefore, F-MoS_2 could achieve an NH_3 yield of 35.7 μg h^{-1} $mg_{cat.}^{-1}$ and a FE of 20.6 %.

Duan et al. prepared an NRR catalyst by completely encapsulating ball-like MoS_2 nanoflowers with a ZIF-71 coating.[84] In this MoS_2@MOF interface, the ZIF-71 coating did not only effectively concentrate N_2 through the inherent micropores, but also acted as a hydrophobic barrier to inhibit the HER process. At the same time, the ball-like MoS_2 nanoflowers provided abundant active edge sites due to the unique ultrathin subunits. Thus, MoS_2@ZIF-71 achieved an NH_3 yield of 56.69 μg h^{-1} mg_{MoS2}^{-1} and a FE of 30.91 %.

4. Theoretical Calculations and Predictions

Since Sun and co-workers used bulk MoS_2 as an electrocatalyst in the N_2 fixation process,[52] a large number of experimental studies on MoS_2-based catalysts have been conducted. In order to facilitate a comparison, performance parameters such as NH_3 production rate and FE were listed in Table 1. Some calculations have also been made to predict the activity of MoS_2-based catalysts, which provided researchers with ideas for enhancing their catalytic activity. So far, calculations and predictions have mainly focused on the heteroatom doping strategies.

Azofra et al. deposited Fe on MoS_2 as an electrocatalyst according to the Fe–Mo–Co structure of nitrogenase.[85] DFT calculations were employed to predict the high selectivity of Fe-MoS_2. Yang et al. used DFT calculations to investigate the NRR activity of some transition metal@MoS_2 systems.[86] By comparing the N_2 adsorption capacity and the potential-determining step (PDS) energy barrier of the selected catalysts, V@MoS_2 was predicted to have the best activity. A DFT theoretical calculation on the performance of MoS_2 doped with transition metals (3d, 4d, 5d elements) was also performed by Zhai et al.[87] Through the metal binding energy (lower than −0.5 eV), they first excluded Zn, Cd and Hg as shown in Figures 7A, B and C. Low metal binging energies indicated weak interactions between metals and substrates. After that, Zr and Ta were also excluded due to the huge distortion. According to the law of free energy variation in the proton coupling, the two highest positive free energy steps ΔG (*N_2—*NNH) and ΔG (*NH_2—*NH_3) needed < 0.49 eV, and only Re and Ti met the requirement as shown in

Table 1. Summary of performance parameters of MoS_2-based catalysts in the NRR process.

Catalyst	Ref.	Electrolyte (Concentration [M])	NH_3 yield rate	FE [%]
MoS_2	[52]	Na_2SO_4 (0.1)	8.08×10^{-11} mol s^{-1} cm^{-1}	1.17
MoS_2 nanoflowers	[53]	Na_2SO_4 (0.1)	29.28 μg h^{-1} $mg_{cat.}^{-1}$	20.8
Ultra-thin MoS_2 nanosheets	[54]	Na_2SO_4 (0.1)	41.66 μg h^{-1} $mg_{cat.}^{-1}$	1.10
PLA-MoS_2	[55]	HCl (0.1)	3405.55 μg h^{-1} $mg_{cat.}^{-1}$	44.36
MoS_2/rGO	[58]	$LiClO_4$ (0.1)	24.82 μg h^{-1} $mg_{cat.}^{-1}$	4.56
MoS_2 nanodots/rGO	[59]	Na_2SO_4 (0.1)	16.41 μg h^{-1} $mg_{cat.}^{-1}$	27.93
MoS_2/g-C_3N_4	[60]	Na_2SO_4 (0.1)	19.86 μg h^{-1} $mg_{cat.}^{-1}$	6.87
1T-MoS_2/g-C_3N_4	[61]	HCl (0.1)	29.97 μg h^{-1} $mg_{cat.}^{-1}$	20.48
1T-MoS_2/BTAB/PPy/GO	[63]	KOH (0.1)	13.60 μg h^{-1} $mg_{cat.}^{-1}$	1.96
1T-MoS_2@Ti_3C_2	[64]	HCl (0.1)	30.33 μg h^{-1} $mg_{cat.}^{-1}$	10.94
Ni-Fe@MoS_2	[65]	Na_2SO_4 (0.1)	128.17 μg h^{-1} $mg_{cat.}^{-1}$	11.34
Fe-MoS_2/CC	[66]	KOH (0.1)	12.5 μg h^{-1} cm^{-2}	10.8
Fe@2H-MoS_2	[67]	HCl (0.1)	n.a.	n.a.
Au NPs@MoS_2	[68]	Na_2SO_4 (0.1)	25 μg h^{-1} $mg_{cat.}^{-1}$	9.7
Ru/2H-MoS_2	[69]	HCl (0.1)	1.14×10^{-10} mol cm^{-2} s^{-1}	17.6
C/MoS_2	[70]	Li_2SO_4 (0.1)	n.a.	8.2
N@MoS_2	[71]	Na_2SO_4 (0.1)	69.82 μg h^{-1} $mg_{cat.}^{-1}$	9.14
B–MoS_2/CFC	[72]	HCl (0.1)	44.09 μg h^{-1} $mg_{cat.}^{-1}$	21.72
FeS@MoS_2/CFC	[73]	Na_2SO_4 (0.1)	8.45 μg h^{-1} cm^{-2}	2.96
CoS_2/MoS_2	[74]	Li_2SO_4 (0.1)	54.7 μg h^{-1} mg^{-1}	20.8
Co–MoS_{2-x}	[75]	H_2SO_4 (0.01)	0.6 mmol h^{-1} g^{-1}	10
Co–MoS_2	[76]	Na_2SO_4 (0.1)	127.88 μg h^{-1} $mg_{cat.}^{-1}$	11.29
Fe-sMoS_2	[77]	HCl (0.1)	24 μg cm^{-2} h^{-1}	27
S-rich MoS_2	[80]	Li_2SO_4 (0.1)	43.4 μg h^{-1} $mg_{cat.}^{-1}$	9.81
1T-MoS_2/NF	[81]	Li_2SO_4 (0.25)	1.05 μg min^{-1} cm^{-2}	27.66
Fe-MoS_2	[82]	K_2SO_4 (0.5)	8.63 μg h^{-1} $mg_{cat.}^{-1}$	18.8
F-MoS_2	[83]	Na_2SO_4 (0.1)	35.7 μg h^{-1} $mg_{cat.}^{-1}$	20.6
MoS_2@ZIF-71	[84]	Na_2SO_4 (0.1)	56.69 μg h^{-1} mg_{MoS2}^{-1}	30.91

© 2021 The Authors. Published by Wiley-VCH GmbH

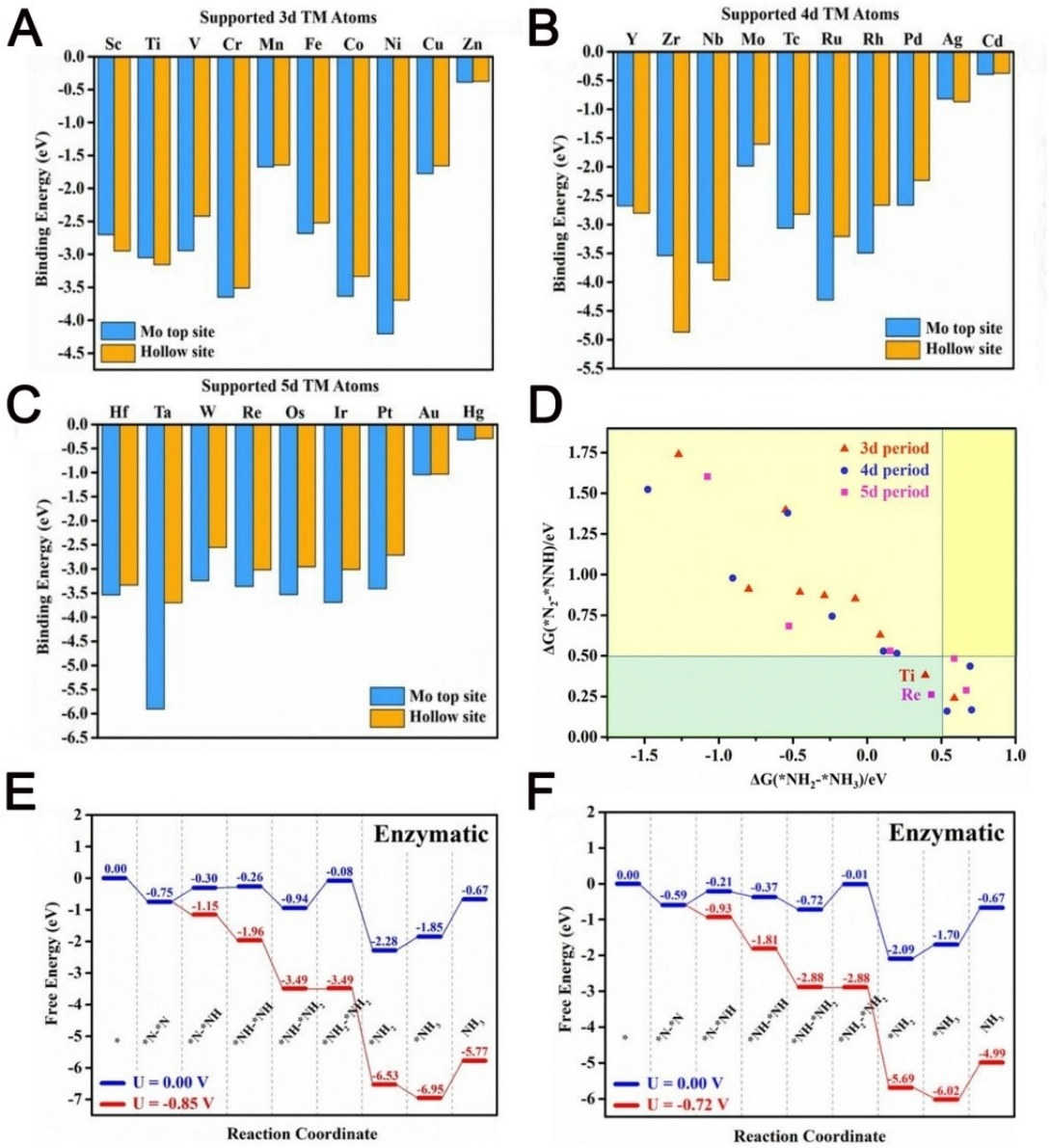

Figure 7. (A–C) The binding energies of 3d, 4d and 5d transition metals (TM) on Mo top sites and hollow sites of MoS_2, respectively. (D) Screening results of TM@MoS_2 systems for the NRR process by the free energy evolution of two thermodynamically detrimental protonation steps ($\Delta G(*N_2–*NNH)$ and $\Delta G(*NH_2–*NH_3)$). The TM@MoS_2 systems which meet the requirement are marked with light cyan color in the lower left part of the graph. (E, F) Enzymatic pathway of side-on adsorbed N_2 molecule on Re@MoS_2 and Ti@MoS_2 for the NRR process, respectively. Reproduced with permission from Ref. [87]. Copyright 2020 Royal Society of Chemistry.

Figure 7D. In the protonation pathway, the PDS energy barrier of Re@MoS_2 (−0.42 eV) was found smaller than that for Ti@MoS_2 (−0.73 eV) (Figure 7E and F). Therefore, Re@MoS_2 was identified as the most suitable catalyst. Moreover, the HER energy barrier of Re@MoS_2 was higher than that for NRR, which proved that Re@MoS_2 was more conducive to N_2 adsorption. The stability of Re@MoS_2 was also demonstrated by ab initio molecular dynamics simulations. Therefore, it seems reasonable to speculate that Re-doped MoS_2 should demonstrate high NRR activities. Zhao et al. also used DFT calculations to predict the NRR activity of some transition metal atoms embedded in MoS_2 nanosheets.[88] The PDS energy barrier of Mo-doped MoS_2 was determined at −0.53 eV (Figure 8A), which was better than other systems. Thus, they regarded Mo/MoS_2 as a potential catalyst for the NRR process.

Although theory predicted encouraging catalytic properties of Mo–MoS_2, Simonov and co-workers recently demonstrated that Mo/MoS_2 was only partially successful in experiments,[89] as the desorption step of NH_3 was not considered. They first carried out an electrocatalytic experiment in water based media (0.1 M Li_2SO_4), but Mo/MoS_2 showed no NRR activity under these conditions (Figure 8B). After that, they experimented with an aprotic medium (1-butyl-1-methylpyrrolidinium (trispenta-

© 2021 The Authors. Published by Wiley-VCH GmbH

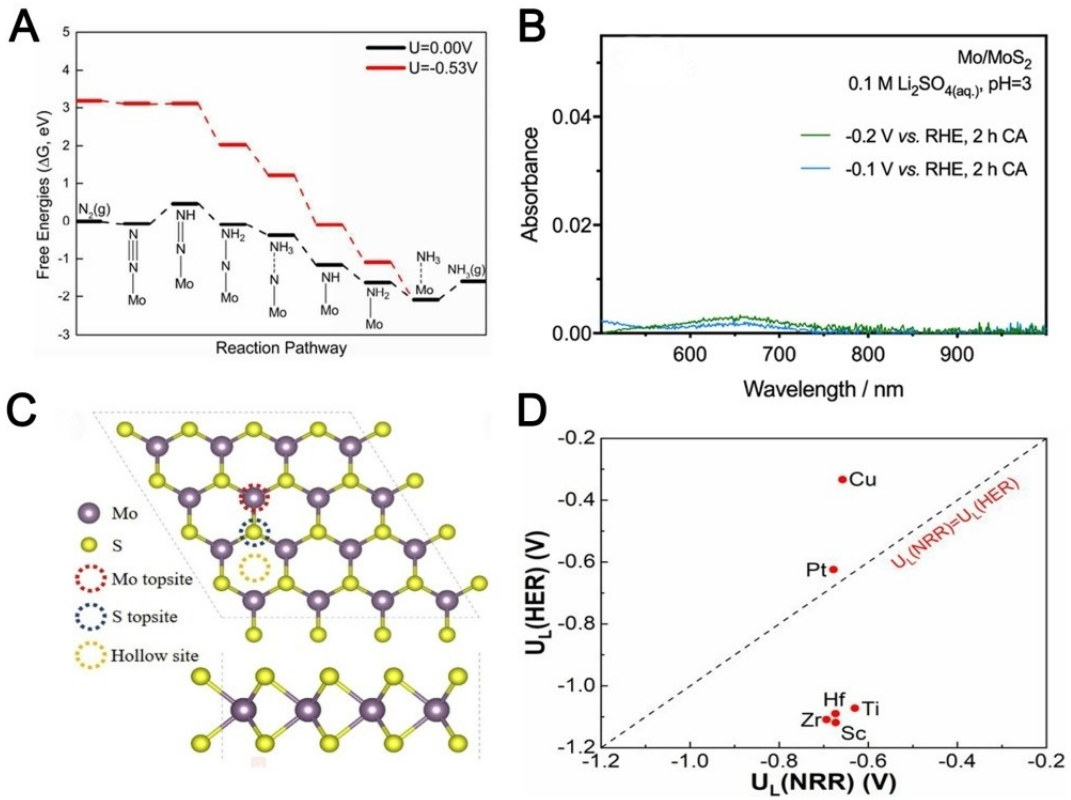

Figure 8. (A) Free energy chart for the NRR process at Mo-doped MoS_2 nanosheets at zero and applied potential (limiting or onset potential). Reproduced with permission from Ref. [88]. Copyright 2018 Royal Society of Chemistry. (B) Berthelot spectrophotometric analysis for ammonium in the working electrolyte solutions after chronoamperometric tests. Reproduced with permission from Ref. [89]. Copyright 2020 Electrochemical Society. (C) Panel views of the Mo top site, the S top site and the hollow site of TM-SAs in the 4×4×1 MoS_2 supercell. Reproduced with permission from Ref. [90]. Copyright 2020 Elsevier. (D) The limiting potentials of HER [UL(HER)] versus NRR [UL (NRR)] on Ti, Cu, Hf, Pt, and Zr-decorated MoS_2. Ti, Cu, Hf, Pt, and Zr-decorated MoS_2 in the region above the dotted line corresponds to HER being more favorable than NRR. Reproduced with permission from Ref. [91]. Copyright 2019 American Chemical Society.

fluoroethyl) trifluorophosphate), in which the water concentration was tightly controlled. At the initial stage of the experiment, the accumulation of NH_3 was stable. However, after more than 2 h of continuous operation, Mo–MoS_2 lost its catalytic activity, because the resulting NH_3/NH_4^+ adsorbed to the surface of Mo–MoS_2, clogging up the active sites. Therefore, it was concluded that the high NRR activity of Mo–MoS_2 predicted by DFT calculations was not feasible in practical experiments even though, through first-principles high-throughput calculations methods, Yang et al. had also predicted the NRR activity of Mo@MoS_2 to be the highest among the calculated systems.[90] In addition, they demonstrated that the N_2 adsorption activity site on the top of Mo atoms had the best NRR performance (Figure 8C). On this basis, other theoretical calculations were adopted to demonstrate high activity and selectivity of Mo@MoS_2–M. However, theoretical prediction lack in investigating the crucial NH_3 desorption step, the high activity of predicted Mo@MoS_2-M still remains to be confirmed experimentally.

Guo et al. aimed at exploring the NRR potential of a part of transition metal-doped (IIIB to IIB subgroups except for Tc and Hg) defective MoS_2.[91] DFT calculations were carried out to affirm the PDS energy barrier of each catalyst; Sc, Ti, Cu, Hf, Pt, and Zr-decorated MoS_2 were considered as potential candidates for N_2 electroreduction to NH_3 due to the PDS energy barrier being smaller than −0.7 eV. To further screen, they tested the limiting potentials of HER [UL(HER)] versus NRR [UL(NRR)] for the six catalyst systems. As shown in Figure 8D, the HER activity of Pt- Cu-modified MoS_2 was higher than N_2 fixation. Thus, Sc, Ti, Hf, and Zr-doped MoS_2 materials were predicted to show a decent NRR activity. Tang and Li predicted that B-doped MoS_2 should have a high NRR catalytic activity,[92] as B is difficult to combine with H under acidic conditions, which could effectively inhibit the HER process. They first contrasted the catalytic properties of B atom- and diatomic boron-doped MoS_2. By calculating overpotentials (0.02 V vs. 0.30 V) and activation barriers (1.24 eV vs. 2.84 eV), they predicted that B_2@MoS_2 should have a better NRR activity. Therefore, defective MoS_2 with double S vacancies was used as substrate to avoid the aggregation of B_2. Meanwhile, the high stability, conductivity and selectivity of B_2@MoS_2 further proved the feasibility of B_2@$MoS_2$for the NRR process, predicting it to be a potentially useful electrocatalyst.

As the synergistic interactions within metal clusters contribute to improving the catalytic activity of individual metal atoms, Zhang et al. attempted to predict the NRR performance of Fe_2/MoS_2 by theoretical calculations.[93] They used DFT calculations combined with the computational hydrogen electrode model,

© 2021 The Authors. Published by Wiley-VCH GmbH

which concluded a high catalytic activity of Fe_2/MoS_2 (the overpotential was 0.21 V and the energy barrier of PDS was −0.37 eV). The catalytic principle of Fe_2/MoS_2 was also proposed (the electron density loss on the Fe cluster provided a stable Lewis active site for the adsorption of N_2, at the same time the electron feedback from the Fe clusters to N_2 promoted the activation of N–N), which further indicated that Fe_2/MoS_2 had potential as a high activity NRR catalyst. Matanovic et al. explored the HER and NRR activity of defect-rich 2H-MoS_2 through experiments and theoretical calculations.[94] By DFT calculations, they predicted that the two vacancies might have NRR selectivity, but FE might not be ideal due to the effect of the large overpotential. Therefore, it was concluded that the original 2H-MoS_2 has a priority role in HER reaction. Further optimization is necessary for 2H-MoS_2 application in the NRR process.

5. Conclusion and Outlook

MoS_2 is considered as a potential NRR catalyst due to the high specific surface area, adjustable electronic structure and elemental composition similar to the nitrogenase enzyme. However, due to the influence of the HER process and the defects of MoS_2, the NRR activity obtained by MoS_2 is not satisfactory. Therefore, optimization of MoS_2 with higher NRR catalytic activity has become a hot research direction. In this Minireview, we summarized the optimization strategies of MoS_2-based catalysts. Optimization strategies include enhancing electrical conductivity/enlarging specific surface area, inhibition of competing reaction and taking advantage of the interaction effect between other elements and MoS_2. In addition, some enhancement strategies by theoretical calculations have also been reviewed, which provides researchers with ideas for enhancing the NRR activity of MoS_2-based catalyst.

Despite some achievements that have been made with MoS_2-based catalysts, it is still a long way from replacing the Haber-Bosch process. Therefore, further optimization is necessary. As MoS_2 is a material with many unique characteristics, optimization research in the future can focus on the characteristics of MoS_2.

(1) It is well known that MoS_2 is a 2D-layered material. The decrease of MoS_2 layer spacing is conducive to inhibit the HER process. Therefore, the NRR selectivity can be improved by reducing the MoS_2 layer gap. Furthermore, ultra-thin mono-layer MoS_2 can observably increase the specific surface area. It is worth considering some other optimization measures on the basis of ultra-thin mono-layer MoS_2.
(2) MoS_2 has a variety of crystal forms (1T, 2H, 3R), among which 1T-MoS_2 and 2H-MoS_2 were widely used in the NRR process. However, the base plane of 2H-MoS_2 is inert, resulting in insufficient adsorption sites. The poor conductivity of 2H-MoS_2 also limits the activity of NRR. Compared with 2H-MoS_2, 1T-MoS_2 shows as an octahedral structure, which not only overcomes the inert base surface to expose a denser active site, but also has high electrical conductivity. Nevertheless, as the inherent HER activity of 1T-MoS_2 is a limitation, future optimization strategies can be developed based on inhibiting the HER activity. Overall, 1T-MoS_2 has the most potential as an efficient catalyst for NRR.
(3) Taking advantage of the characteristic of the adjustable electronic structure of MoS_2, the electrical conductivity and N_2 adsorption capacity can be improved by changing the electronic structure of MoS_2.
(4) As N_2 is dissolved in water during the NRR process, it is converted to NH_3 in contact with the catalyst surface. However, the intrinsic surface of MoS_2 is hydrophobic,[95] which prevents N_2 from contacting the surface of the catalyst. Thus, taking measures to change the hydrophobicity of MoS_2-based catalysts is also a potential research area.

Acknowledgements

This work was supported by the Young Taishan Scholars Program of Shandong Province (tsqn201909124), the National Natural Science Foundation of China (21775054), the Project of "20 items of University" of Jinan (2019GXRC018) and the National Key Scientific Instrument and Equipment Development Project of China (21627809). All of authors express their sincere thanks.

Conflict of Interest

The authors declare no conflict of interest.

Keywords: ambient NH_3 synthesis · electrocatalysis · electrochemical N_2 reduction reaction · MoS_2 · optimization strategies

[1] D. W. Boukhvalov, *Phys. Chem. Chem. Phys.* **2015**, *17*, 27210–27216.
[2] M. Duca, M. T. M. Koper, *Energy Environ. Sci.* **2012**, *5*, 9726.
[3] R. F. Service, *Science.* **2014**, *345*, 610.
[4] J. Zhao, X. Ren, X. Li, D. Fan, X. Sun, H. Ma, Q. Wei, D. Wu, *Nanoscale* **2019**, *11*, 4231–4235.
[5] A. Klerke, C. H. Christensen, J. K. Nørskov, T. Vegge, *J. Mater. Chem.* **2008**, *18*, 2304–2310.
[6] S. Mekhilef, R. Saidur, A. Safari, *J. Renew. Sustain. Ener.* **2012**, *16*, 981–989.
[7] C. Guo, J. Ran, A. VasileffS, S. Qiao, *Energy Environ. Sci.* **2018**, *11*, 45–56.
[8] C. J. M. van der Ham, M. T. M. Koper, D. G. H. Hetterscheid, *Chem. Soc. Rev.* **2014**, *43*, 5183–5191.
[9] P. Wei, Q. Geng, A. I. Channa, X. Tong, Y. Luo, S. Lu, G. Chen, S. Gao, Z. Wang, X. Sun, *Nano Res.* **2020**, *13*, 2967–2972.
[10] C. Wang, J. Gao, J. Zhao, D. Yan, X. Zhu, *Small* **2020**, 16, 1907091.
[11] X. Zhu, S. Mou, Q. Peng, Q. Liu, Y. Luo, G. Chen, S. Gao, X. Sun, *J. Mater. Chem. A* **2020**, *8*, 1545–1556.
[12] L. Zhang, M. Cong, X. Ding, Y. Jin, F. Xu, Y. Wang, L. Chen, L. Zhang, *Angew. Chem. Int. Ed.* **2020**, *59*, 10888–10893; *Angew. Chem.* **2020**, *132*, 10980–10985.
[13] J. Zhao, L. Zhang, X. Xie, X. Li, Y. Ma, Q. Liu, W. Fang, X. Shi, G. Cui, X. Sun, *J. Mater. Chem. A* **2018**, *6*, 24031–24035.
[14] Y. Chen, R. Guo, X. Peng, X. Wang, X. Liu, J. Ren, J. He, L. Zhuo, J. Sun, Y. Liu, Y. Wu, J. Luo, *ACS Nano* **2020**, *14*, 6938–6946.
[15] L. Zhao, J. Zhou, L. Zhang, X. Sun, X. Sun, T. Yan, X. Ren, Q. Wei, *ACS Appl. Mater. Interfaces* **2020**, *12*, 55838–55843.

© 2021 The Authors. Published by Wiley-VCH GmbH

[16] W. Cai, Y. Han, Y. Pan, X. Zhang, J. Xu, Y. Zhang, Y. Sun, S. Li, J. Lai, L. Wang, *J. Mater. Chem. A* **2021**, *9*, 13483–13489.
[17] H. Tao, C. Choi, L.-X. Ding, Z. Jiang, Z. Han, M. Jia, Q. Fan, Y. Gao, H. Wang, A. W. Robertson, S. Hong, Y. Jung, S. Liu, Z. Sun, *Chem.* **2019**, *5*, 204–214.
[18] H. Wang, S. Liu, H. Zhang, S. Yin, Y. Xu, X. Li, Z. Wang, L. Wang, *Nanoscale* **2020**, *12*, 13507–13512.
[19] X. Xu, X. Liu, J. Zhao, D. Wu, Y. Du, T. Yan, N. Zhang, X. Ren, Q. Wei, *J. Colloid Interface Sci.* **2021**, *606*, 1374–1379.
[20] Z. Wu, R. Zhang, H. Fei, R. Liu, D. Wang, X. Liu, *Appl. Surf. Sci.* **2020**, *532*, 147372.
[21] J. Zhao, B. Wang, Q. Zhou, H. Wang, X. Li, H. Chen, Q. Wei, D. Wu, Y. Luo, J. You, F. Gong, X. Sun, *Chem. Commun.* **2019**, *55*, 4997–5000.
[22] L. Li, H. Chen, L. Li, B. Li, Q. Wu, C. Cui, B. Deng, Y. Luo, Q. Liu, T. Li, F. Zhang, A. M. Asiri, Z. Feng, Y. Wang, X. Sun, *Chin. J. Catal.* **2021**, *42*, 1755–1762.
[23] Y. Liu, Y. Luo, Q. Li, J. Wang, K. Chu, *Chem. Commun.* **2020**, *56*, 10227–10230.
[24] Z. Du, J. Liang, S. Li, Z. Xu, T. Li, Q. Liu, Y. Luo, F. Zhang, Y. Liu, Q. Kong, X. Shi, B. Tang, A. M. Asiri, B. Li, X. Sun, *J. Mater. Chem. A* **2021**, *9*, 13861–13866.
[25] S. Zhang, C. Zhao, Y. Liu, W. Li, J. Wang, G. Wang, Y. Zhang, H. Zhang, H. Zhao, *Chem. Commun.* **2019**, *55*, 2952–2955.
[26] W. Kong, F. Gong, Q. Zhou, G. Yu, L. Ji, X. Sun, A. M. Asiri, T. Wang, Y. Luo, Y. Xu, *J. Mater. Chem. A* **2019**, *7*, 18823–18827.
[27] F. Wang, Y. P. Liu, H. Zhang, K. Chu, *ChemCatChem* **2019**, *11*, 1441–1447.
[28] J. Zhao, J. Yang, L. Ji, H. Wang, H. Chen, Z. Niu, Q. Liu, T. Li, G. Cui, X. Sun, *Chem. Commun.* **2019**, *55*, 4266–4269.
[29] S. Zhang, G. Duan, L. Qiao, Y. Tang, Y. Chen, Y. Sun, P. Wan, S. Zhang, *Ind. Eng. Chem. Res.* **2019**, *58*, 8935–8939.
[30] Q. Liu, T. Xu, Y. Lou, Q. Kong, T. Li, S. Lu, A. A. Alshehri, K. A. Alzahrani, X. Sun, *Curr. Opin. Electrochem.* **2021**, *29*, 100766.
[31] X. Cheng, J. Wang, W. Xiong, T. Wang, T. Wu, S. Lu, G. Chen, S. Gao, X. Shi, Z. Jiang, X. Niu, X. Sun, *ChemNanoMat* **2020**, *6*, 1315–1319.
[32] X. Lv, Y. Liu, Y. Wang, X. Liu, Z. Yuan, *Appl. Catal. B* **2021**, *280*, 119434.
[33] X. Chen, K. Li, X. Yang, J. Lv, S. Sun, S. Li, D. Cheng, B. Li, Y. Li, H. Zang, *Nano Res.* **2020**, *14*, 501–506.
[34] T. Wu, H. Zhao, X. Zhu, Z. Xing, Q. Liu, T. Liu, S. Gao, S. Lu, G. Chen, A. M. Asiri, Y. Zhang, X. Sun, *Adv. Mater.* **2020**, *32*, e2000299.
[35] X. Zhu, J. Zhao, L. Ji, T. Wu, T. Wang, S. Gao, A. A. Alshehri, K. A. Alzahrani, Y. Luo, Y. Xiang, B. Zheng, X. Sun, *Nano Res.* **2019**, *13*, 209–214.
[36] N. Cao, Z. Chen, K. Zang, J. Xu, J. Zhong, J. Luo, X. Xu, G. Zheng, *Nat. Commun.* **2019**, *10*, 2877.
[37] T. Xu, J. Liang, Y. Wang, S. Li, Z. Du, T. Li, Q. Liu, Y. Luo, F. Zhang, X. Shi, B. Tang, Q. Kong, A. M. Asiri, C. Yang, D. Ma, X. Sun, *Nano Res.* **2021**, DOI: 10.1007/s12274-021-3592-8.
[38] Y. Zhang, W. Qiu, Y. Ma, Y. Luo, Z. Tian, G. Cui, F. Xie, L. Chen, T. Li, X. Sun, *ACS Catal.* **2018**, *8*, 8540–8544.
[39] X. Ren, J. Zhao, Q. Wei, Y. Ma, H. Guo, Q. Liu, Y. Wang, G. Cui, A. M. Asiri, B. Li, B. Tang, X. Sun, *ACS Cent. Sci.* **2019**, *5*, 116–121.
[40] Y. P. Liu, Y. B. Li, D. J. Huang, H. Zhang, K. Chu, *Chem.* **2019**, *25*, 11933–11939.
[41] S. Li, Y. Lan, L. Yue, T. Li, Y. Wang, Q. Liu, G. Cui, F. Zhang, A. M. Asiri, X. Sun, *Chem. Commun.* **2021**, *57*, 7806–7809.
[42] J. Zhao, X. Liu, X. Ren, X. Sun, D. Tian, Q. Wei, D. Wu, *Appl. Catal. B* **2021**, *284*, 119746.
[43] G. F. Chen, X. Cao, S. Wu, X. Zeng, L. X. Ding, M. Zhu, H. Wang, *J. Am. Chem. Soc.* **2017**, *139*, 9771–9774.
[44] H. Chen, J. Liang, L. Li, B. Zheng, Z. Feng, Z. Xu, Y. Luo, Q. Liu, X. Shi, Y. Liu, S. Gao, A. M. Asiri, Y. Wang, Q. Kong, X. Sun, *ACS Appl. Mater. Interfaces* **2021**, *13*, 41715–41722.
[45] X. Ren, G. Cui, L. Chen, F. Xie, Q. Wei, Z. Tian, X. Sun, *Chem. Commun.* **2018**, *54*, 8474–8477.
[46] X. Zhu, Z. Liu, H. Wang, R. Zhao, H. Chen, T. Wang, F. Wang, Y. Luo, Y. Wu, X. Sun, *Chem. Commun.* **2019**, *55*, 3987–3990.
[47] C. Suresh, S. Mutyala, J. Mathiyarasu, *Mater. Lett.* **2016**, *164*, 417–420.
[48] I. S. Amiinu, Z. Pu, X. Liu, K. A. Owusu, H. G. R. Monestel, F. O. Boakye, H. Zhang, S. Mu, *Adv. Funct. Mater.* **2017**, *27*, 1702300.
[49] C. Lee, S. Ozden, C. S. Tewari, O. K. Park, R. Vajtai, K. Chatterjee, P. M. Ajayan, *ChemSusChem* **2018**, *11*, 2960–2966.
[50] H. Zhang, Y. Tian, J. Zhao, Q. Cai, Z. Chen, *Electrochim. Acta* **2017**, *225*, 543–550.
[51] Z. Luo, Y. Ouyang, H. Zhang, M. Xiao, J. Ge, Z. Jiang, J. Wang, D. Tang, X. Cao, C. Liu, W. Xing, *Nat. Commun.* **2018**, *9*, 2120.
[52] L. Zhang, X. Ji, X. Ren, Y. Ma, X. Shi, Z. Tian, A. M. Asiri, L. Chen, B. Tang, X. Sun, *Adv. Mater.* **2018**, *30*, 1800191.
[53] X. Li, T. Li, Y. Ma, Q. Wei, W. Qiu, H. Guo, X. Shi, P. Zhang, A. M. Asiri, L. Chen, B. Tang, X. Sun, *Adv. Energy Mater.* **2018**, *8*, 1801357.
[54] Y. Liao, W. Ye, Y. Zhu, L. Wang, *Int. J. Electrochem. Sci.* **2020**, *15*, 11555–11566.
[55] J. Chen, C. Zhang, M. Huang, J. Zhang, J. Zhang, H. Liu, G. Wang, R. Wang, *Appl. Catal. B* **2021**, *285*, 119810.
[56] Q. H. Wang, K. Kalantar-Zadeh, A. Kis, J. N. Coleman, M. S. Strano, *Nat. Nanotechnol.* **2012**, *7*, 699–712.
[57] Y. Liang, H. Wang, J. Zhou, Y. Li, J. Wang, T. Regier, H. Dai, *J. Am. Chem. Soc.* **2012**, *134*, 3517–3523.
[58] X. Li, X. Ren, X. Liu, J. Zhao, X. Sun, Y. Zhang, X. Kuang, T. Yan, Q. Wei, D. Wu, *J. Mater. Chem. A* **2019**, *7*, 2524–2528.
[59] Y. Liu, W. Wang, S. Zhang, W. Li, G. Wang, Y. Zhang, M. Han, H. Zhang, *ACS Sustainable Chem. Eng.* **2020**, *8*, 2320–2326.
[60] Z. Zhao, S. Luo, P. Ma, Y. Luo, W. Wu, Y. Long, J. Ma, *ACS Sustainable Chem. Eng.* **2020**, *8*, 8814–8822.
[61] X. Xu, X. Tian, B. Sun, Z. Liang, H. Cui, J. Tian, M. Shao, *Appl. Catal. B* **2020**, *272*, 118984.
[62] M. A. Lukowski, A. S. Daniel, F. Meng, A. Forticaux, L. Li, S. Jin, *J. Am. Chem. Soc.* **2013**, *135*, 10274–10277.
[63] H. Mao, Y. Fu, H. Yang, Z. Z. Deng, Y. Sun, D. Liu, Q. Wu, T. Ma, X. M. Song, *ACS Appl. Mater. Interfaces* **2020**, *12*, 25189–25199.
[64] X. Xu, B. Sun, Z. Liang, H. Cui, J. Tian, *ACS Appl. Mater. Interfaces* **2020**, *12*, 26060–26067.
[65] L. Zeng, X. Li, S. Chen, J. Wen, W. Huang, A. Chen, *J. Mater. Chem. A* **2020**, *8*, 7339–7349.
[66] X. Zhao, X. Zhang, Z. Xue, W. Chen, Z. Zhou, T. Mu, *J. Mater. Chem. A* **2019**, *7*, 27417–27422.
[67] J. Guo, T. Tadesse Tsega, I. Ul Islam, A. Iqbal, J. Zai, X. Qian, *Chin. Chem. Lett.* **2020**, *31*, 2487–2490.
[68] Y. Zhou, X. Yu, X. Wang, C. Chen, S. Wang, J. Zhang, *Electrochim. Acta* **2019**, *317*, 34–41.
[69] B. H. R. Suryanto, D. Wang, L. M. Azofra, M. Harb, L. Cavallo, R. Jalili, D. R. G. Mitchell, M. Chatti, D. R. MacFarlane, *ACS Energy Lett.* **2018**, *4*, 430–435.
[70] L. Duan, Y. Guohua, L. Nan, A. Z. Abdullah, *E3S Web Conf.* **2021**, *245*, 03022.
[71] L. Zeng, S. Chen, J. van der Zalm, X. Li, A. Chen, *Chem. Commun.* **2019**, *55*, 7386–7389.
[72] Y. Guo, Z. Yao, S. Zhan, B. J. J. Timmer, C. Tai, X. Li, Z. Xie, Q. Meng, L. Fan, F. Zhang, M. S. G. Ahlquist, M. Cuartero, G. A. Crespo, L. Sun, *Nano Energy* **2020**, *78*, 105391.
[73] Y. Guo, Z. Yao, B. J. J. Timmer, X. Sheng, L. Fan, Y. Li, F. Zhang, L. Sun, *Nano Energy* **2019**, *62*, 282–288.
[74] G. Yang, L. Zhao, G. Huang, Z. Liu, S. Yu, K. Wang, S. Yuan, Q. Sun, X. Li, N. Li, *ACS Appl. Mater. Interfaces* **2021**, *13*, 21474–21481.
[75] J. Zhang, X. Tian, M. Liu, H. Guo, J. Zhou, Q. Fang, Z. Liu, Q. Wu, J. Lou, *J. Am. Chem. Soc.* **2019**, *141*, 19269–19275.
[76] L. Zeng, X. Li, S. Chen, J. Wen, F. Rahmati, J. van der Zalm, A. Chen, *Nanoscale* **2020**, *12*, 6029–6036.
[77] J. Zheng, S. Wu, L. Lu, C. Huang, P. Ho, A. Kirkland, T. Sudmeier, R. Arrigo, D. Gianolio, S. C. Edman Tsang, *Chem. Sci.* **2021**, 12, 688–695.
[78] F. Jiao, B. Xu, *Adv. Mater.* **2019**, *31*, 1805173.
[79] T. Oshikiri, K. Ueno, H. Misawa, *Angew. Chem. Int. Ed.* **2016**, *55*, 3942–3946; *Angew. Chem.* **2016**, *128*, 4010–4014.
[80] Y. Liu, M. Han, Q. Xiong, S. Zhang, C. Zhao, W. Gong, G. Wang, H. Zhang, H. Zhao, *Adv. Energy Mater.* **2019**, *9*, 1803935.
[81] S. B. Patil, H. Chou, Y. Chen, S. H. Hsieh, C. Chen, C. Chang, S. Li, Y. C. Lee, Y. Lin, H. Li, Y. Chang, Y. Lai, D. Wang, *J. Mater. Chem. A* **2021**, *9*, 1230–1239.
[82] H. Su, L. Chen, Y. Chen, R. Si, Y. Wu, X. Wu, Z. Geng, W. Zhang, J. Zeng, *Angew. Chem. Int. Ed.* **2020**, *59*, 20411–20416; *Angew. Chem.* **2020**, *132*, 20591–20596.
[83] J. Liang, S. Ma, J. Li, Y. Wang, J. Wu, Q. Zhang, Z. Liu, Z. Yang, K. Qu, W. Cai, *J. Mater. Chem. A* **2020**, *8*, 10426–10432.
[84] J. Duan, D. Shao, X. He, Y. Lu, W. Wang, *Colloids Surf. A* **2021**, *619*, 126529.
[85] L. M. Azofra, C. Sun, L. Cavallo, D. R. MacFarlane, *Chem.* **2017**, *23*, 8275–8279.
[86] L. Yang, F. Chen, E. Song, Z. Yuan, B. Xiao, *ChemPhysChem* **2020**, *21*, 1235–1242.
[87] X. Zhai, L. Li, X. Liu, Y. Li, J. Yang, D. Yang, J. Zhang, H. Yan, G. Ge, *Nanoscale* **2020**, *12*, 10035–10043.

© 2021 The Authors. Published by Wiley-VCH GmbH

[88] J. Zhao, J. Zhao, Q. Cai, *Phys. Chem. Chem. Phys.* **2018**, *20*, 9248–9255.
[89] H.-L. Du, R. Y. Hodgetts, M. Chatti, C. K. Nguyen, D. R. MacFarlane, A. N. Simonov, *J. Electrochem. Soc.* **2020**, *167*, 146507.
[90] T. Yang, T. T. Song, J. Zhou, S. Wang, D. Chi, L. Shen, M. Yang, Y. P. Feng, *Nano Energy* **2020**, *68*, 104304.
[91] H. Guo, L. Li, X. Wang, G. Yao, H. Yu, Z. Tian, B. Li, L. Chen, *ACS Appl. Mater. Interfaces* **2019**, *11*, 36506–36514.
[92] F. Li, Q. Tang, *Nanoscale* **2019**, *11*, 18769–18778.
[93] H. Zhang, C. Cui, Z. Luo, *J. Phys. Chem. C* **2020**, *124*, 6260–6266.
[94] I. Matanovic, K. Leung, S. J. Percival, J. E. Park, P. Lu, P. Atanassov, S. S. Chou, *Appl. Mater. Res.* **2020**, *21*, 100812.
[95] Y. Song, Z. Jiang, B. Gao, H. Wang, M. Wang, Z. He, X. Cao, F. Pan, *Chem. Eng. Sci.* **2018**, *185*, 231–242.

Manuscript received: August 20, 2021
Revised manuscript received: September 28, 2021

© 2021 The Authors. Published by Wiley-VCH GmbH